Supporting Information

Mitigating Metal Dendrite Formation in Lithium–Sulfur Batteries via Morphology–Tunable Graphene Oxide Interfaces

Yu-Ting Chen,[†] Syed Ali Abbas,[‡,†] Nahid Kaisar,[∃,†] Sheng Hui Wu,[∥] Hsin-An Chen,[†] Karunakara Moorthy Boopathi,[†] Mriganka Singh,[†,§] Jason Fang,[∥] Chun-Wei Pao,[†] and Chih-Wei Chu*[,†,¶,±]

[†] *Research Center of Applied Sciences, Academia Sinica, Taipei 115, Taiwan*

[¶] *College of Engineering, Chang Gung University, Guishan District, Taoyuan City 33302, Taiwan*

[±] *Department of Materials Science and Engineering, National Tsing Hua University, Hsinchu 30013, Taiwan*

[‡] *Department of Engineering and Systems Science, National Tsing Hua University, Hsinchu 30013, Taiwan*

[§] *Department of Materials Science and Engineering, National Chiao Tung University, Hsinchu 30010, Taiwan*

[∥] *Material and Chemical Research Laboratories, Industrial Technology Research Institute, Hsinchu 31040, Taiwan*

[∃] *Department of Materials Science and Engineering, National Taiwan University of Science and Technology, Taipei 106, Taiwan*

*To whom correspondence should be addressed: E-mail gchu@gate.sinica.edu.tw

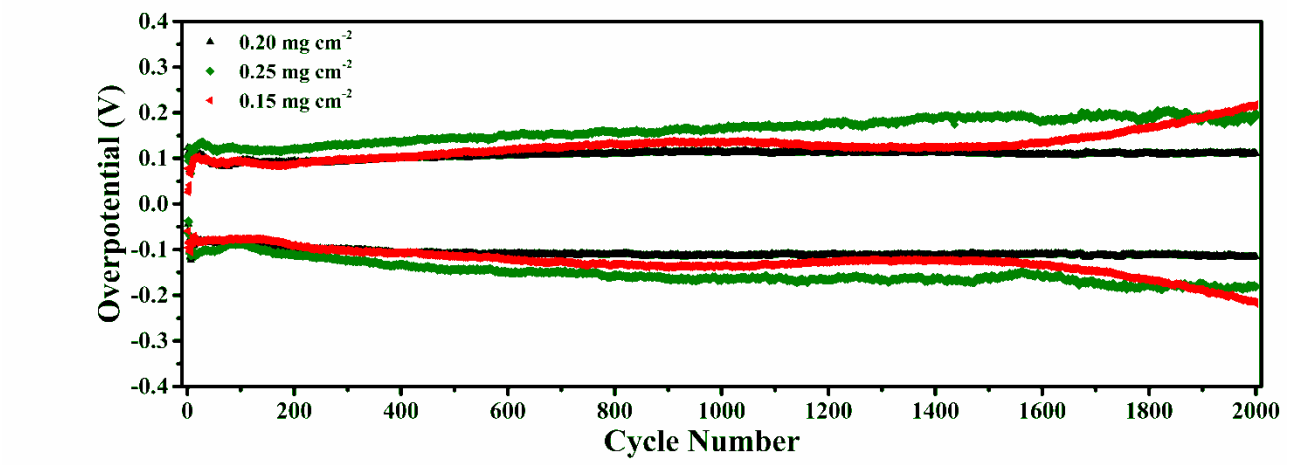

Figure S1. Overpotentials plotted with respect to the cycle number for D-GO-Li symmetrical cells featuring various GO loadings, tested at a current density of 5 mA cm^{-2} and a deposition capacity of 1 mA h cm^{-2} for 2000 cycles.

Note: Figure S1 presents the overpotential profiles of D-GO-Li symmetrical cells featuring various GO loadings. When GO loading was 0.15 mg cm^{-2}, the cell exhibited a slightly lower overpotential, relative to prepared at 0.2 mg cm^{-2}, prior to 200 cycles, and maintained a similar overpotential up to 1400 cycles. Nevertheless, the thinner coating led to the stability being lost after 1400 cycles, and the overpotential increased rapidly. At a loading of 0.25 mg cm^{-2}, although the sample maintained its stability for the duration of the test, the overpotential was substantially higher from the onset, due to a higher resistance resulting from the thicker coating. Hence, a coating of 0.20 mg cm^{-2} was considered the optimized thickness.

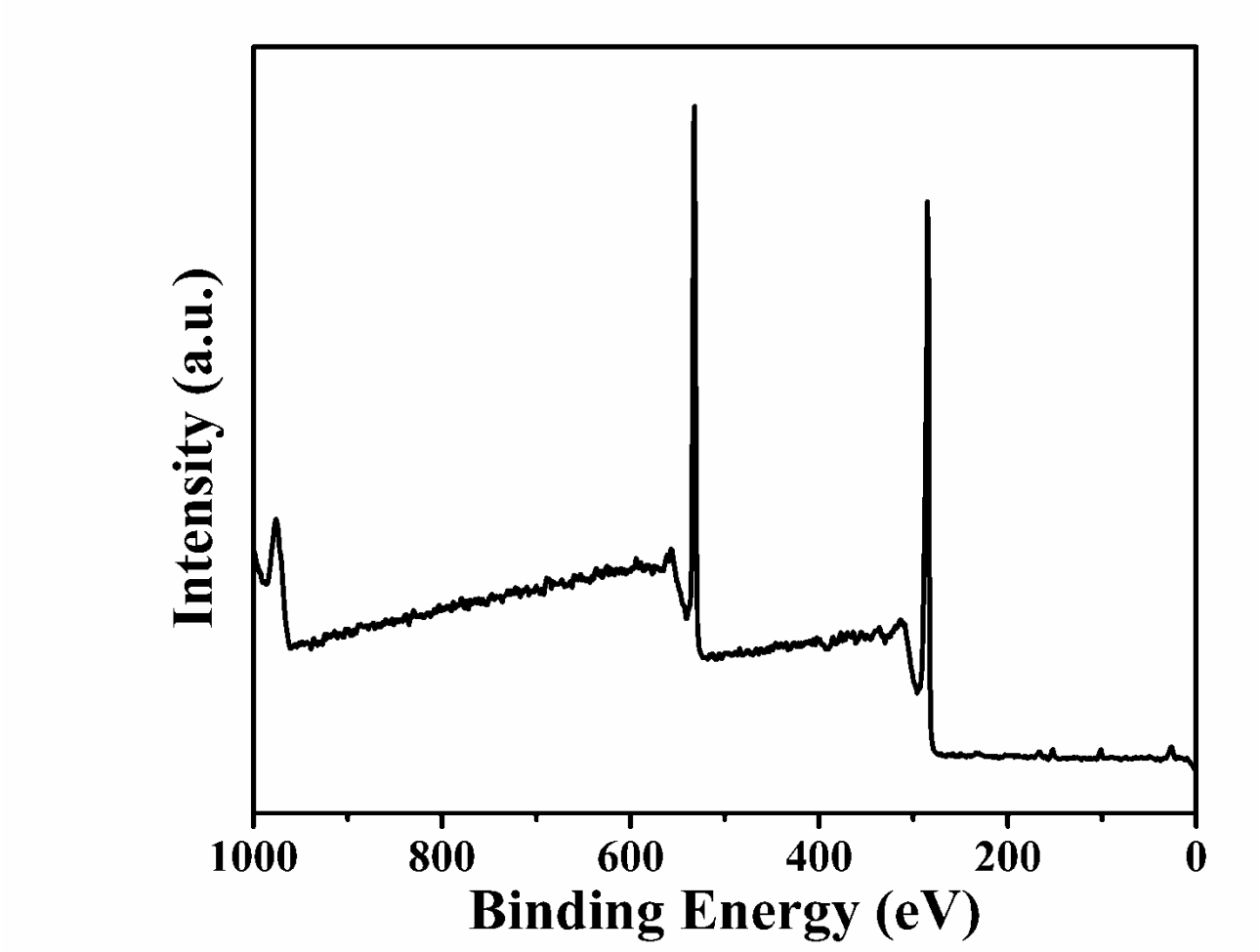

Figure S2. XPS full spectrum of GO (C:O atomic ratio: 4:1).

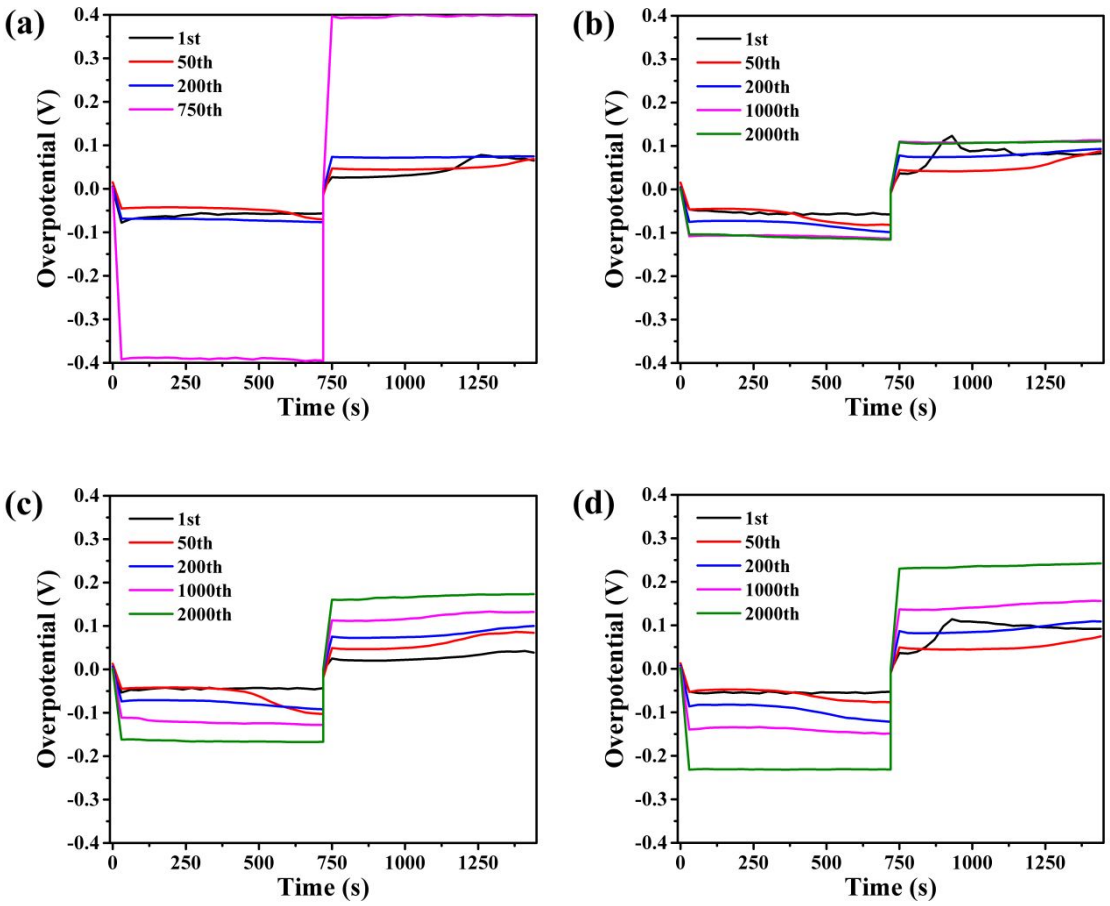

Figure S3. Overpotential profiles for (a) B-Li, (b) D-GO-Li, (c) D-GOAl-Li and (d) S-GO-Li from the selected cycles of symmetrical cell tests.

Table S1. Fitted values of EIS

sample	R_S	R_{CT}	CPE-T_{CT}	CPE-P_{CT}	R_D	CPE-T_D	CPE-P_D
B-Li	2.9	82.4	1.19×10^{-5}	8.26×10^{-1}	27	5.4×10^{-3}	7.7×10^{-1}
D-GO-Li	4.95	33	1.32×10^{-4}	7.13×10^{-1}	172	7.0×10^{-3}	4.8×10^{-1}
D-GOAl-Li	3.4	19	7.3×10^{-5}	7.0×10^{-1}	140	7.6×10^{-3}	5.1×10^{-1}
S-GO-Li	9.6	4	8.12×10^{-5}	9.06×10^{-1}	122	1.09×10^{-2}	4.5×10^{-1}
Al_2O_3 only	2.3	255	1.06×10^{-5}	8.27×10^{-1}	74	4.4×10^{-3}	8.9×10^{-1}

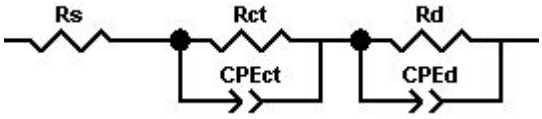

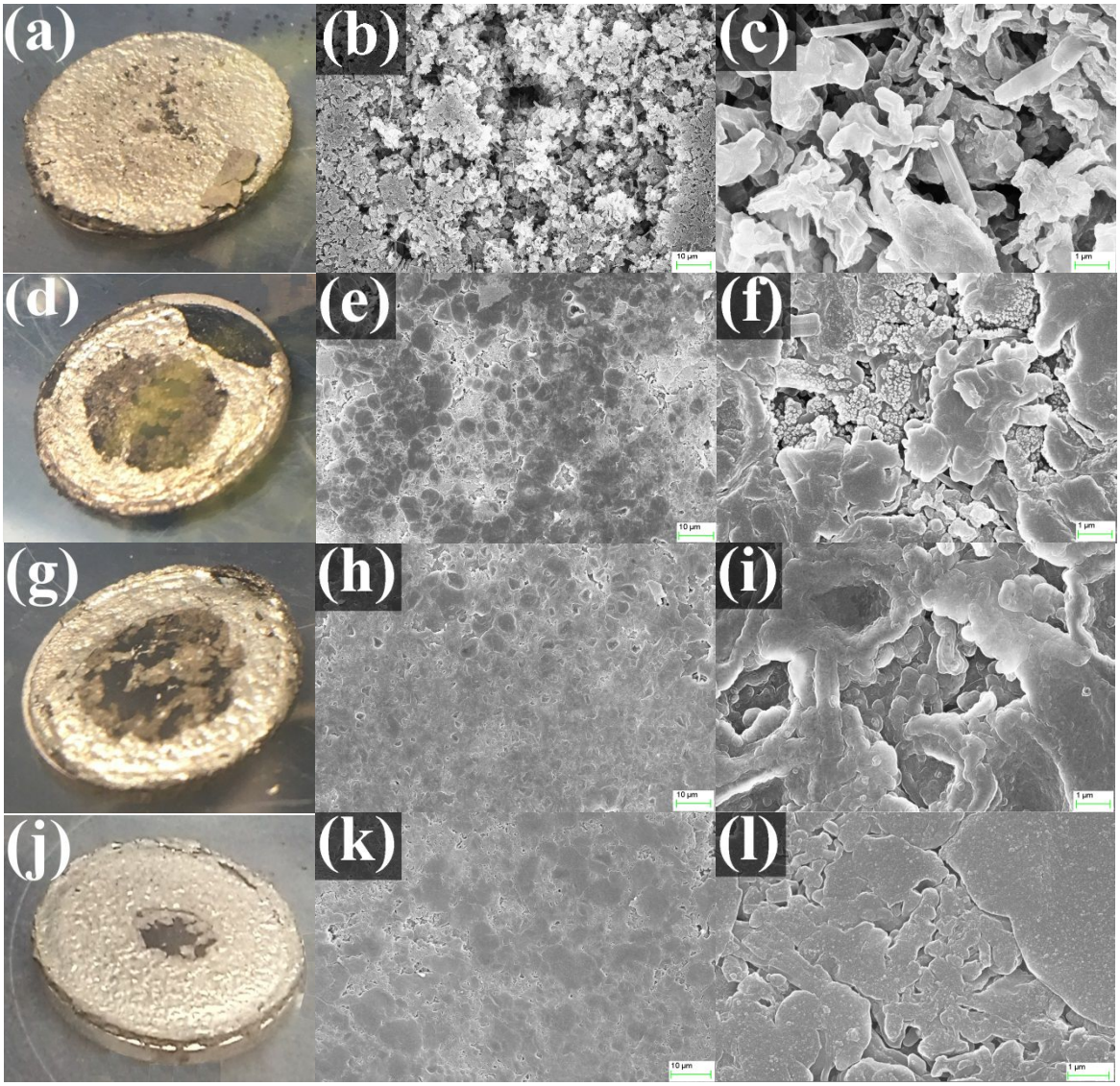

Figure S4. Optical (a, d, g, j) and SEM (b, c, e, f, h, i, k, l) images of Li metal anodes after symmetrical cell tests performed at a current density of 5 mA cm^{-2} and a deposition capacity of 1 mA h cm^{-2} over 2000 cycles. (a–c) B-Li, (d–f) D-GO-Li, (g–i) D-GOAl-Li, and (j–l) S-GO-Li.

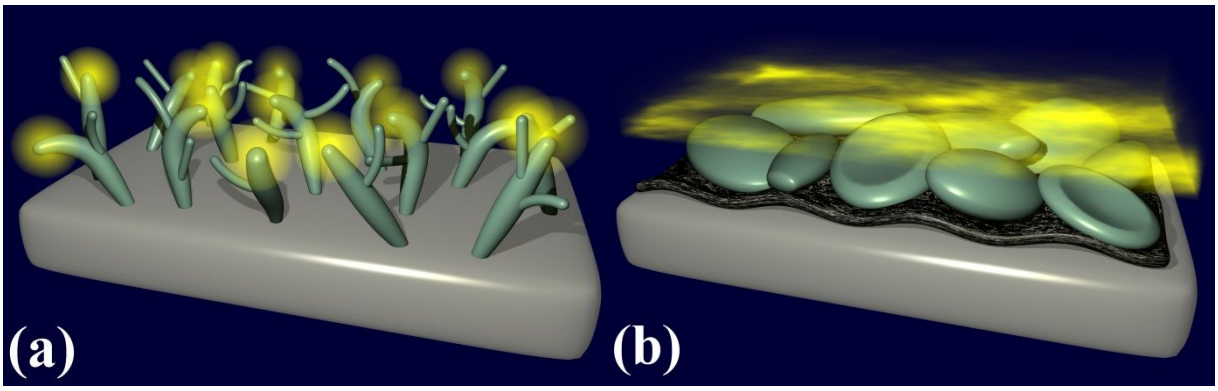

Figure S5. Schematic representations of Li metal anodes. (a) Without a GO coating, the Li metal anodes are more inclined to form needle-like dendrites with sharp tips at which the electric field (yellow mist) could concentrate; such a concentrated electric field would further encourage dendrite formation. (b) With GO coatings, the Li deposited without forming sharp tips, and the concentration electric field was avoided.

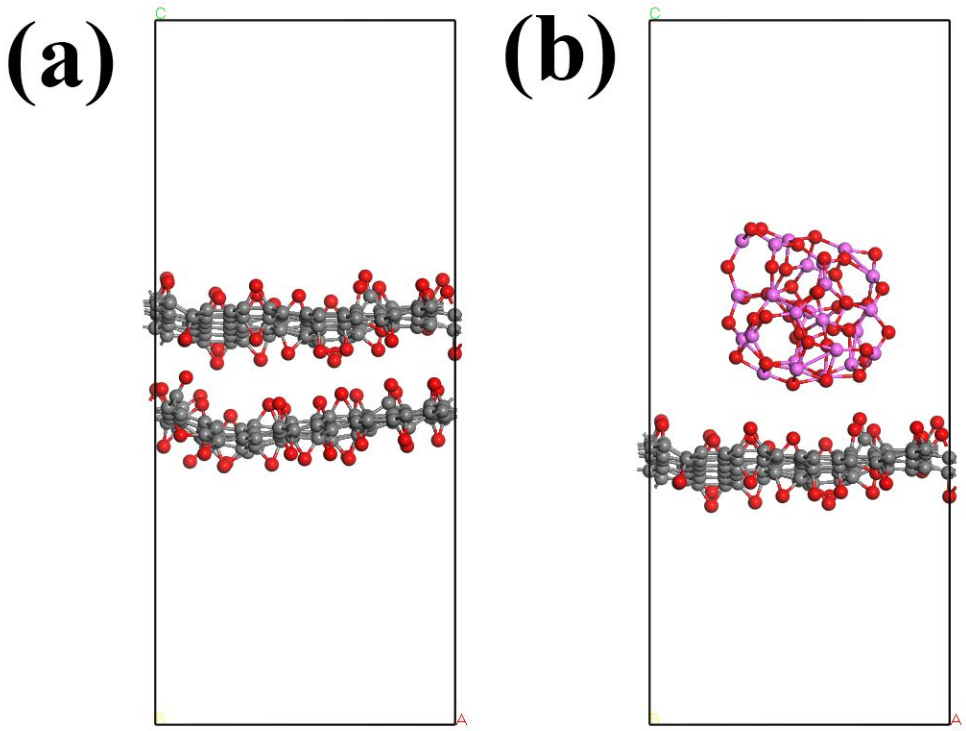

Figure S6. Interactions within (a) GO–GO and (b) GO–Al_2O_3 structures (binding energies: –1.797 and –3.959 eV, respectively).

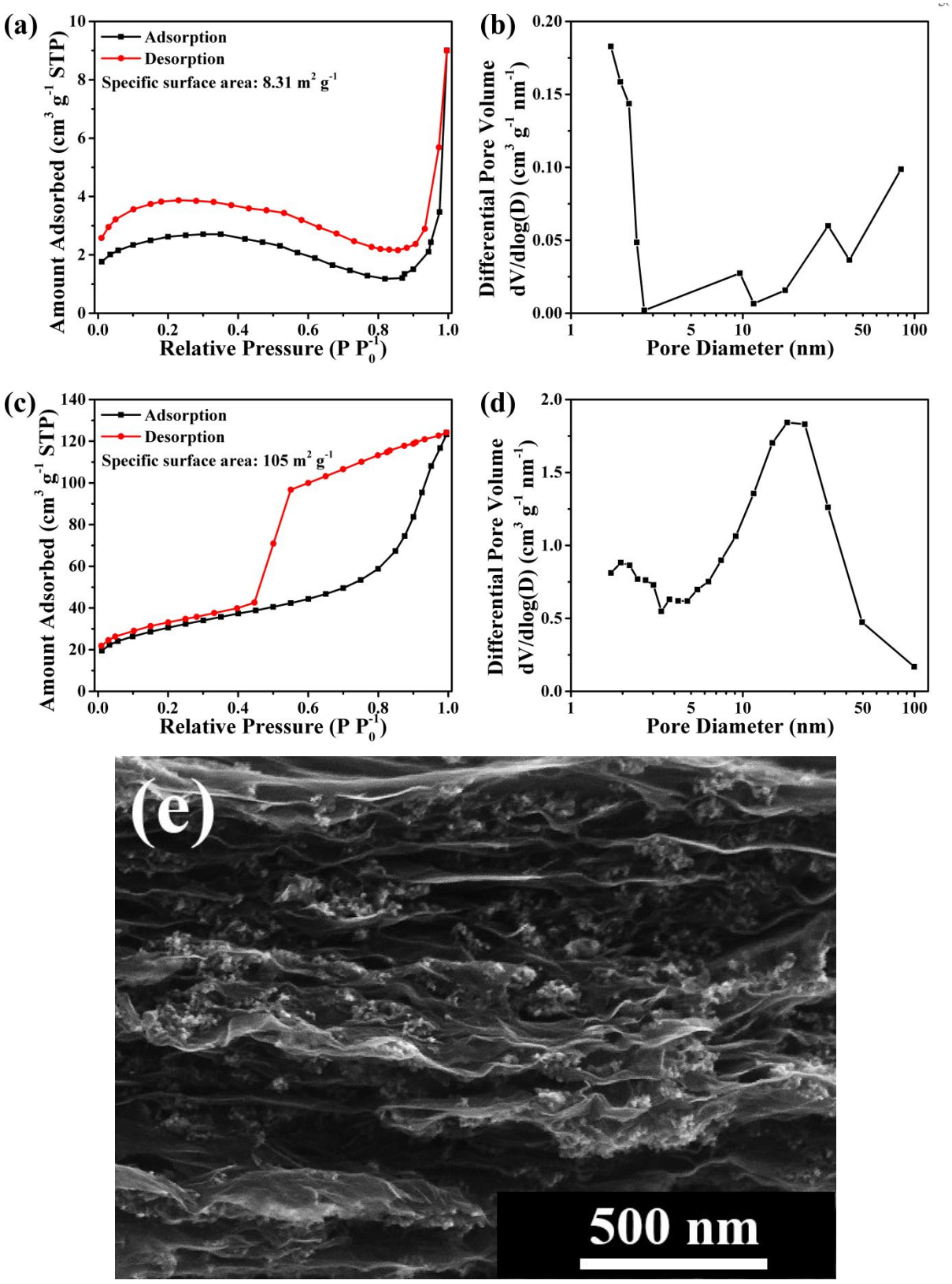

Figure S7. The (a, c) adsorption–desorption isotherms and (b, d) pore size distribution of (a, b) GO and (c, d) GO–Al_2O_3 powder. (e) The enlarged SEM image of GO–Al_2O_3 coating.

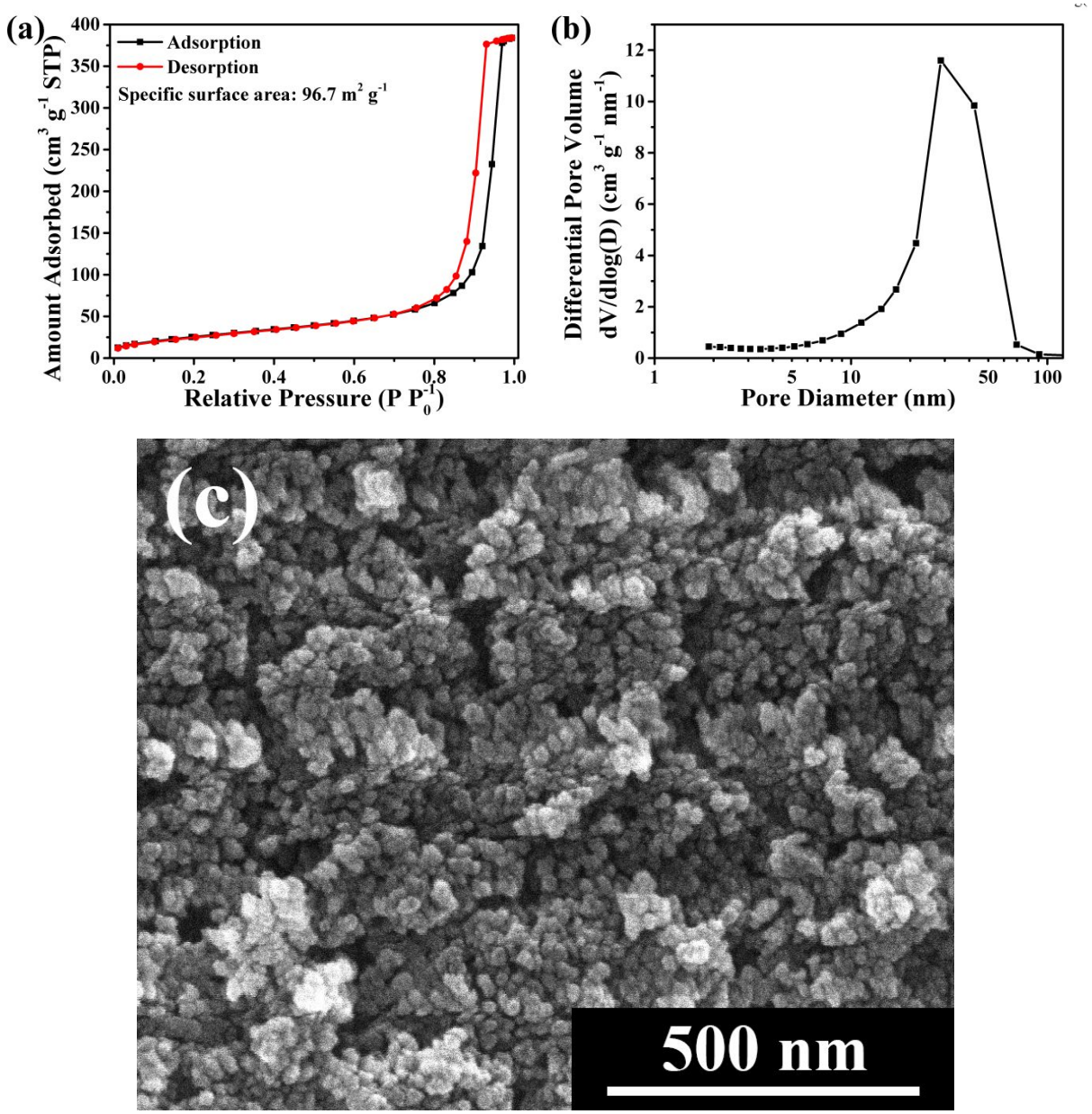

Figure S8. The (a) adsorption–desorption isotherms, (b) pore size distribution and (c) SEM image of Al_2O_3 nanoparticle powder.

Note: Although Al_2O_3 nanoparticles show similar BET surface area to GO–Al_2O_3, the isotherm and pore size distribution were different. Al_2O_3 nanoparticle exhibited a much narrower capillary condensation desorption hysteresis and a sharper pore size peak than GO–Al_2O_3. In SEM image, pores constructed by nanoparticles with more consistent size than that of GO–Al_2O_3 were observed. Moreover, GO–Al_2O_3 consisted of GO : Al_2O_3 with a weight ratio of 2 : 1 and its BET surface area was not the linear combination of GO and Al_2O_3 nanoparticles (37.8 m^2 g^{-1}), implying that the surface area of GO–Al_2O_3 was not contributed by any single material, but by synergistic effect between GO layers and Al_2O_3 nanoparticles.

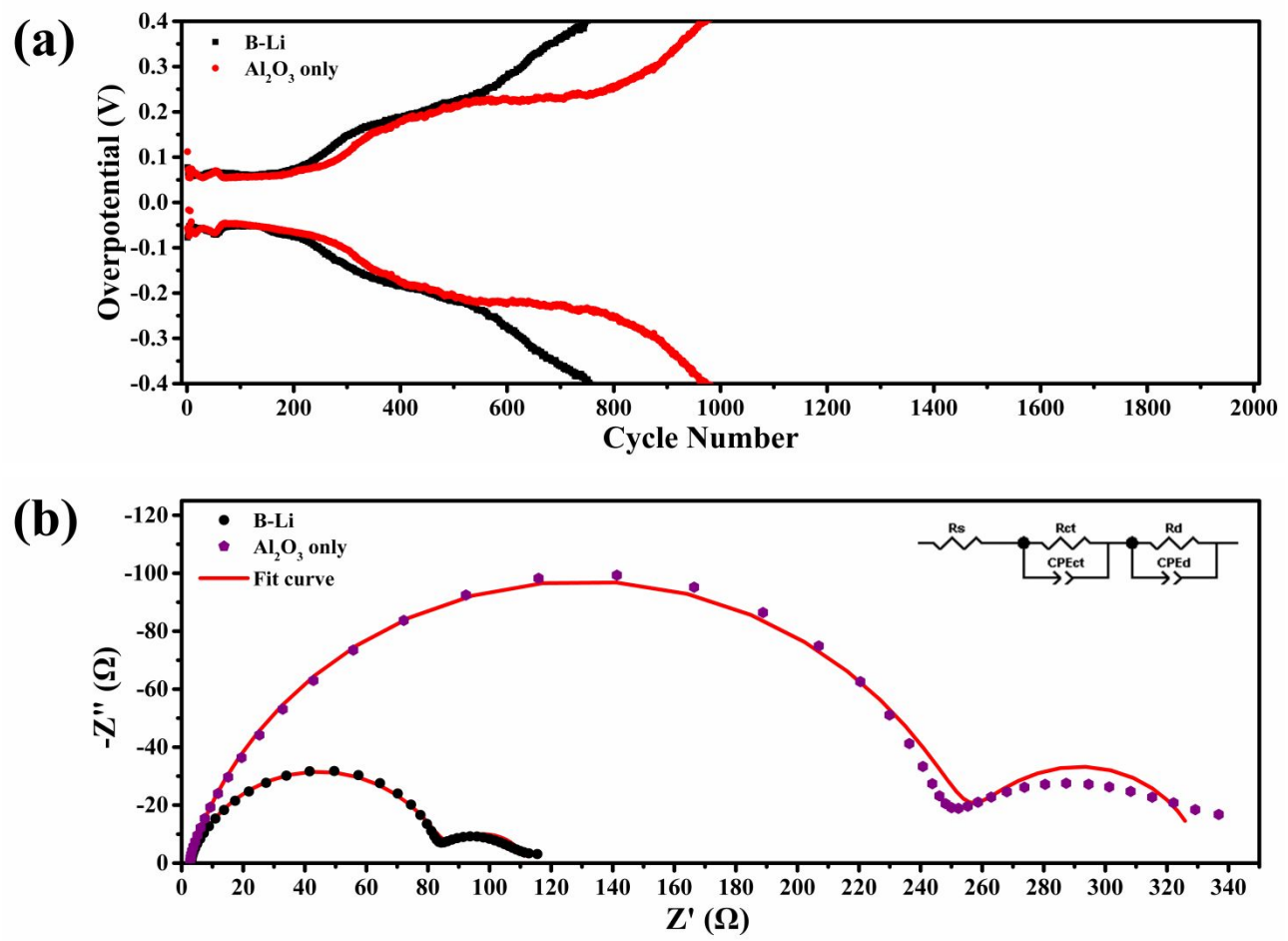

Figure S9. (a) Polarization plotted with respect to the cycle number for B-Li and Al_2O_3-coated Li anode symmetrical cells, tested at a current density of 5 mA cm^{-2} and a deposition capacity of 1 mA h cm^{-2} for 2000 cycles. (b) The AC impedance and the circuit employed for fitting.

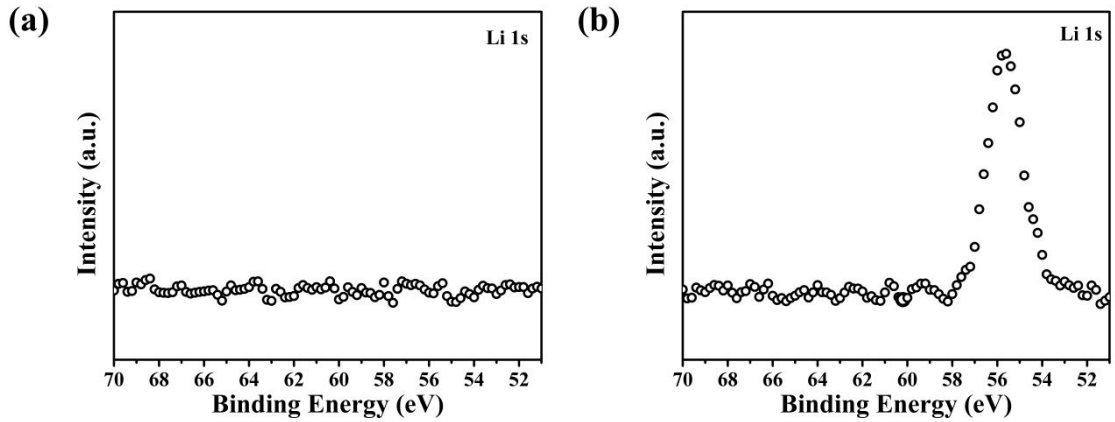

Figure S10. Li 1s XPS spectra of GO (a) before and (b) after discharging.

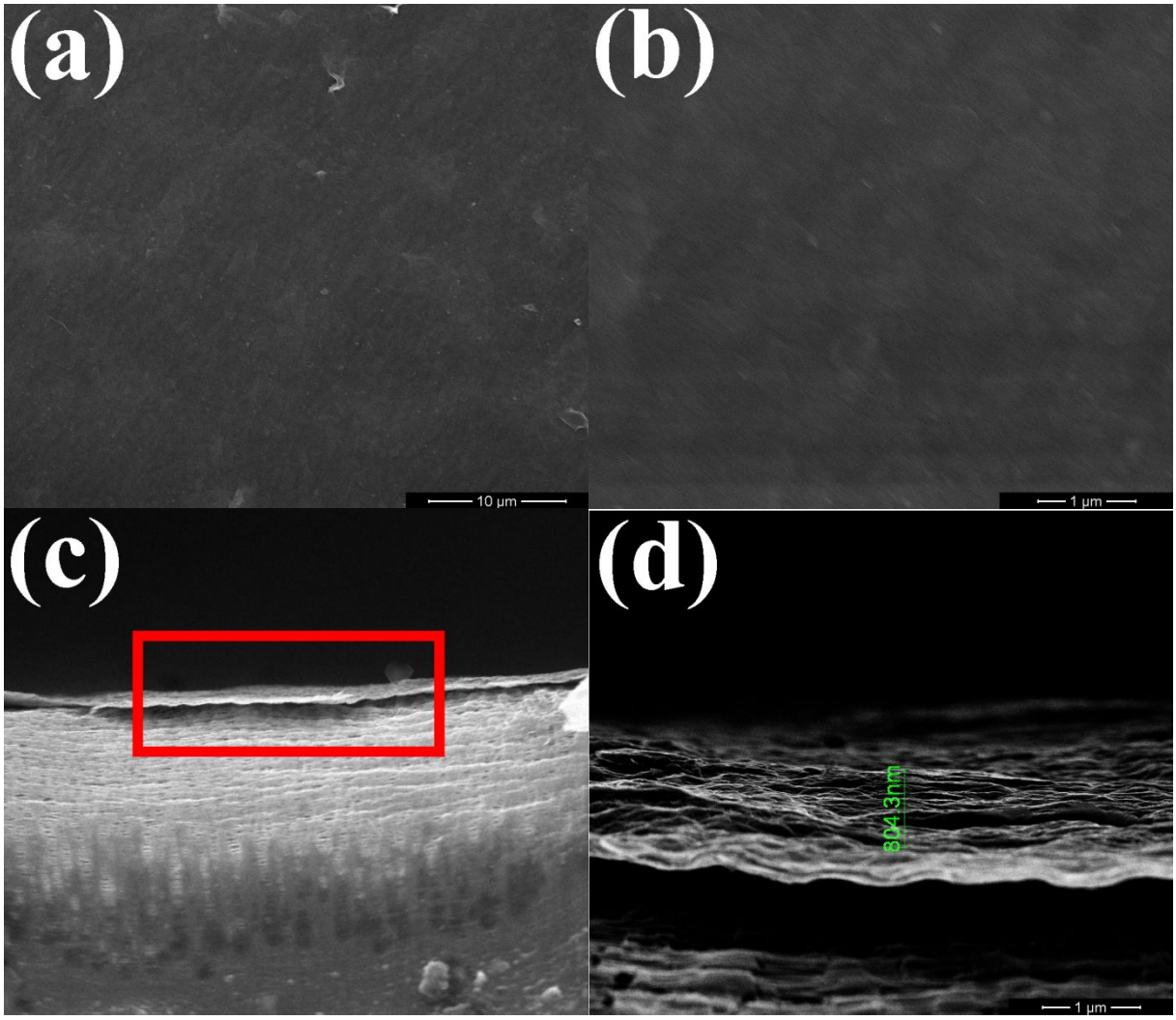

Figure S11. (a, b) Top-view and (c-d) cross-sectional SEM images of the GO layer on a coated separator.

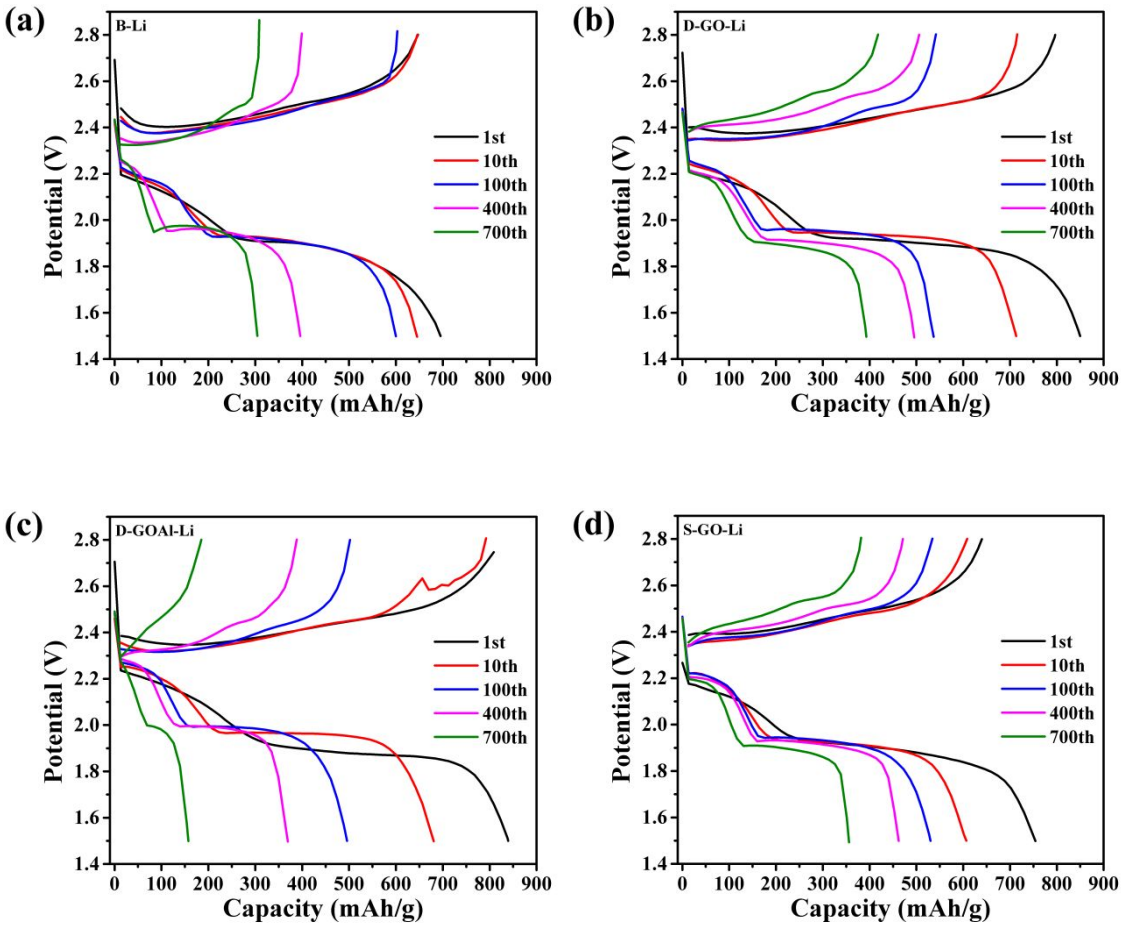

Figure S12. Charge-discharge curves for (a) B-Li, (b) D-GO-Li, (c) D-GOAl-Li and (d) S-GO-Li from the selected cycles of Li-S cell tests.

Movie S1 The complete plating process for the B-Li transparent cell.

Movie S2 The complete plating process for the D-GO-Li transparent cell.